Supporting information

Stress acidulated amphoteric molecules and mechanochromism via reversible intermolecular proton transfer

Yi Wang,[a] Minjie Li,[*,a] Yumo Zhang,[a] Jin Yang,[b] Shaoyin Zhu,[a] Lan Sheng,[a] Xudong Wang,[a] Bing Yang[a] and Sean Xiao-An Zhang[*,a]

[a] *State Key Lab of Supramolecular Structure and Materials, College of Chemistry, Jilin University, Changchun 130012, People's Republic of China*

[b] *Key Lab of Polyoxometalate Science, Department of Chemistry, Northeast Normal University, Changchun 130024, People's Republic of China*

Table of Contents

1. Experimental details

1.1 Materials

Phenylhydrazine, 3-methylbutan-2-one and salicylaldehyde were purchased from commercial sources and used without further purification. 3-nitrosalicylaldehyde, 5-nitrosalicylaldehyde, 3,5-dinitrosalicylaldehyde and 2,3,3-trimethyl-3H-indole were synthesized according to literature procedures.[1]

1.2 Characterization

^{1}H NMR (500 MHz) and ^{13}C NMR (126 MHz) spectra were recorded on a Bruker AVANCE500 using TMS as a standard at room temperature. ^{1}H NMR (300 MHz) and ^{13}C NMR (75 MHz) spectra were recorded on a Varian Mercury using TMS as a standard at room temperature. LC-HRMS analysis was performed on an Agilent 1290-microTOF-Q II mass spectrometer. UV-Vis absorption spectra were measured using a Shimadzu UV-2550 PC double-beam spectrophotometer. Fluorescence experiments were performed on a Shimadzu RF-5301 PC spectrofluorimeter. Reflection spectroscopy was performed on a Maya 2000PRO fiber optical spectrometer with Ocean DH-2000-BAL UV-Vis-NIR light source using $BaSO_4$ as background. Then they were converted to Kubelka-Munk diffuse reflectance absorption spectra using Kubelka-Munk function.[2] True-color fluorescence images were obtained by using an Olympus microscope (BX-51) equipped with a digital color camera and a broad-band ultraviolet (330-385 nm) light source (100W mercury lamp). IR spectra studies were performed on Vertex 80/80V FT-IR spectrometer with LN-MCT Mid DC detector over the range of 4000-800 cm^{-1} using a KBr plate. X-ray Photoelectron Spectroscopy (XPS) measurements were carried out under condition of 15 kV and 17 mA using a Thermo ESCALAB 250 spectrometer with a twin-anode Al·Kα (1486.6 eV) X-ray source. DSC experiments were recorded on a NETZSCH DSC 204 instrument at a scanning rate of 10 $K \cdot min^{-1}$. Single-crystal X-ray diffraction data for **AM** was recorded on a Rigaku RAXIS-PRID diffractometer using the ω-scan mode with graphite-monochromator Mo·Kα radiation (λ = 0.71073 Å). Single-crystal X-ray diffraction data for **p-nitro-AM** and **o-nitro-AM** were recorded on a Bruker-AXS Smart CCD diffractometer, using ω-scan technique with Cu·Kα radiation (λ = 1.5418 Å). The structures were solved with direct methods using the SHELXTL programs and refined with full-matrix least squares on F^2. Powder X-ray diffraction measurements were performed on Rigaka D-max 2550 diffractometer with the Cu·Kα (λ = 1.5418 Å) radiation under a scan step of 0.02 degree.

Mechanical stress was avoided to apply on the unground samples. The powdery unground samples for reflectance, fluorescence, XPS and XRD measurements were all purified by column chromatography and dried with a vacuum rotary evaporator. The gathering of the sample from the flask was mainly by shaking and knocking the flask without using spatula to press the sample. The unground sample for IR measurement was prepared by dropping the dichloromethane solution of corresponding compounds onto the surface of blank KBr plates, and measurements were performed after samples were fully dried under infrared lamp. Samples for reflectance, fluorescence, XPS, and XRD

measurements were all prepared by putting the powdery samples on the sample holders without any press and the sample holders were all placed horizontally for the measurements.

The NBO analysis[3] was employed to calculate the charge distribution of **AM**, **p-nitro-AM** and **o-nitro-AM** in twisted and planar conformations using the density functional theory (DFT) with RB3LYP hybrid functional at the basis set level of 6-31G (d, p). The twisted conformations were obtained directly from their crystal structures. Their planar conformations were obtained in the following step. First, the conformations obtained from the crystal were fully optimized using RB3LYP/6-31G (d, p). Then frequency calculations were performed at the same level of theory to ensure that the systems represent true minima on the potential energy surfaces. UV-Vis and IR spectra of neutral and zwitterionic isomers of **AM**, **p-nitro-AM** and **o-nitro-AM** and total energies for the isolated neutral and zwitterionic isomers of **p-nitro-AM** were simulated with the same methods. All the theoretical calculations were performed using Gaussian 09 package.[4]

1.3 Synthesis

1.3.1 Synthesis of AM

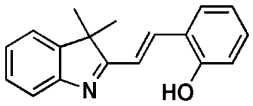

Compounds of 2,3,3-trimethyl-3H-indole (0.320 g, 2.0 mmol) and salicylaldehyde (0.370 g, 3.0 mmol) were refluxed in anhydrous alcohol solution (15 ml) for 27 hours. The mixture was then concentrated under reduced pressure, and the residue was purified by column chromatography [SiO_2: hexane / ethyl acetate (20:1)] to afford **AM** (0.230 g, 44%) as a yellow solid. LC-HRMS: m/z calcd. $[M + H]^+$ 264.1383, found 264.1380. ^{1}H NMR (500 MHz, DMSO-d_6), δ (TMS, ppm): 10.09 (s, 1H), 8.01 (d, J = 16.5, 1H), 7.75 (d, J = 7.4, 1H), 7.51 (d, J = 7.6, 1H), 7.46 (d, J = 7.2, 1H), 7.30 (t, 1H), 7.24-7.18 (m, 3H), 6.92 (d, J = 8.1, 1H), 6.86 (t, 1H), 1.38 (s, 6H). ^{13}C NMR (126 MHz, DMSO-d_6), δ (TMS, ppm): 184.00, 156.61, 154.30, 147.03, 133.31, 130.98, 128.03, 127.96, 125.60, 123.04, 121.92, 120.31, 119.86, 119.17, 116.52, 52.60, 23.57, 23.57.

1.3.2 Synthesis of p-nitro-AM

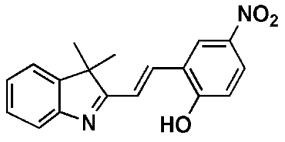

Compounds of 2,3,3-trimethyl-3H-indole (0.180 g, 1.1 mmol) and 5-nitrosalicylaldehyde (0.242 g, 1.4 mmol) were refluxed in anhydrous alcohol solution (20 ml) for 10.5 hours. Then the mixture was concentrated under reduced pressure, the residue was purified by column chromatography [SiO_2: hexane / ethyl acetate (12:1)] to afford **p-nitro-AM** (0.196 g, 58%) as a yellow solid. LC-HRMS: m/z calcd. $[M + H]^+$ 309.1239, found 309.1240. ^{1}H NMR (500 MHz, DMSO-d_6), δ (TMS, ppm): 11.74 (s, 1H), 8.70 (d, J = 2.5 Hz, 1H), 8.12 (dd, J = 9.0, 2.6 Hz, 1H), 7.99 (d, J = 16.4 Hz, 1H), 7.55-7.47 (m, 3H), 7.33 (t, 1H), 7.23 (t, 1H), 7.09 (d, J = 9.0 Hz, 1H), 1.41 (s, 6H). ^{13}C NMR (126 MHz, DMSO-d_6), δ (TMS, ppm):183.73, 162.40, 154.11, 147.17, 140.59, 130.99, 128.11, 126.34, 126.00, 124.08, 123.79, 122.02, 122.02, 120.63, 116.87, 52.85, 23.19, 23.19.

1.3.3 Synthesis of o-nitro-AM

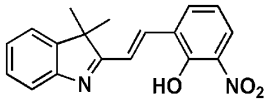

Compounds of 2,3,3-trimethyl-3H-indole (0.575 g, 3.6 mmol) and a mixture of 5-nitrosalicylaldehyde and 3-nitrosalicylaldehyde (0.505 g, 3.0 mmol) were refluxed in anhydrous alcohol solution (20 ml) for 8 hours. Then the mixture was concentrated under reduced pressure, the residue was purified by column chromatography [SiO_2: hexane / ethyl acetate (10:1)] to afford **p-nitro-AM** (0.110 g, 12%) and **o-nitro-AM** (0.220 g, 24%) as a yellow solid. LC-HRMS: m/z calcd. $[M + H]^+$ 309.1234, found 309.1227. ^{1}H NMR (500 MHz, DMSO-d_6), δ (TMS, ppm): 10.94 (s, 1H), 8.27 (d, J = 7.6, 1H), 8.08 (d, J = 16.4, 1H), 8.03 (d, J = 8.2, 1H), 7.57 (d, J = 7.6, 1H), 7.49 (d, J = 7.2, 1H), 7.39 (d, J = 16.4, 1H), 7.34 (t, 1H), 7.25 (t, 1H), 7.14 (t, 1H), 1.41 (s, 6H).^{13}C NMR (126 MHz, DMSO-d_6), δ (TMS, ppm): 183.45, 154.04, 151.13, 147.09, 137.19, 134.12, 130.35, 128.16, 127.89, 126.12, 126.12, 122.16, 122.05, 120.74, 120.34, 52.83, 23.27, 23.27.

1.3.4 Synthesis of di-nitro-AM

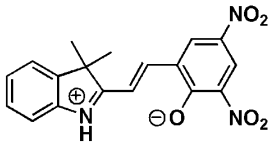

Compounds of 2,3,3-trimethyl-3H-indole (0.209 g, 1.3 mmol) and 3, 5-dinitrosalicylaldehyde (0.213 g, 1.0 mmol) were refluxed in an anhydrous alcohol solution (10 ml) for 7 hours. After cooling down to ambient temperature, black red precipitation was filtered off and washed with ethanol for several times to afford **di-nitro-AM** (0.307 g, 87%) as a black red solid. LC-HRMS: m/z calcd. $[M + H]^+$ 354.1084, found 354.1072. ^{1}H NMR (500 MHz, DMSO-d_6), δ (TMS, ppm): 8.74 (d, J = 3.1, 1H), 8.57 (d, J = 3.1, 1H), 8.36 (d, J = 16.0, 1H), 8.17 (d, J = 16.0, 1H), 7.74 (d, J = 6.6, 1H), 7.56-7.43 (m, 3H), 1.66 (s, 6H). ^{13}C NMR (75 MHz, DMSO-d_6), δ (TMS, ppm): 186.05, 168.44, 148.15, 144.02, 142.01, 140.73, 132.93, 129.32, 129.08, 127.87, 126.91, 125.25, 123.29, 116.21, 112.79, 52.36, 24.36, 24.36.

1.3.5 Synthesis of 6-N-BIPS

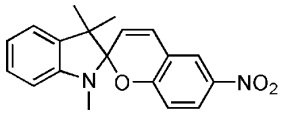

6-N-BIPS was synthesized according to literature procedures.[5] LC-HRMS: m/z calcd. $[M + H]^+$ 323.1390, found 323.1389. ^{1}H NMR (300 MHz, $CDCl_3$) δ (TMS, ppm): 8.04-8.00 (m, 2H), 7.21 (t, 1H), 7.10 (d, J = 6.0, 1H), 6.95-6.86 (m, 2H), 6.77 (d, J = 10.3, 1H), 6.56 (d, J = 7.8, 1H), 5.86 (d, J = 10.3, 1H), 2.74 (s, 3H), 1.30 (s, 3H), 1.19 (s, 3H).

2. Density functional theory (DFT) calculations for AM, p-nitro-AM and o-nitro-AM and X-Ray crystallographic analyses for AM, p-nitro-AM and o-nitro-AM

Table S1. NBO charge distribution of **AM**，**p-nitro-AM** and **o-nitro-AM** in twisted (T) and planar (P) conformations.

NBO charge	H in O-H	N in C=N
AM (T)	0.456	-0.453
AM (P)	0.497	-0.448
p-nitro-AM (T)	0.460	-0.441
p-nitro-AM (P)	0.503	-0.434
o-nitro-AM (T)	0.478	-0.422
o-nitro-AM (P)	0.524	-0.422

The natural bond orbital (NBO) charge analysis shows clearly the obvious difference in charge distribution between twisted and planar conformations for **AM**, **p-nitro-AM** and **o-nitro-AM**. For instance, the NBO charge of its phenolic proton (0.497) in **AM** for the optimized planar structure is bigger than that for the twisted one (0.456), suggesting a stronger acidity in a planar conformation. Meanwhile, the basicity for planar conformation is slightly lower than that for twisted one from the decreasing NBO charge distribution for nitrogen. Overall, the enhancement of electropositivity for phenolic proton is eight times larger than the reduction of electronegativity for nitrogen in indole group, which means acidic enhancement is dominating during a transition from twisted to planar conformation. The same results are also observed for **p-nitro-AM** and **o-nitro-AM**.

Figure S1. Simulated UV-Vis and IR spectra of neutral and zwitterionic isomers for **AM**, **p-nitro-AM** and **o-nitro-AM**.

The simulated UV-Vis absorption results indicate that the neutral-to-zwitterionic transition gives rise to a drastic bathochromic shift in UV-Vis spectra with the maximum absorption peak red-shifted about 100 nm. The trend is consistent with experimental data, in which the absorption bandedge red-shifted about 100 nm after proton transfer.

The simulated IR spectra results indicate the stretching absorption of O–H will disappear with the appearance of the stretching absorption of N–H, and the stretching absorption in 500-1750 cm^{-1} will have a dramatic intensity increment. Both results are consistent with the experimental data.

Because the calculation is dealing with a single molecule in vacuum, which differs from experimental conditions, it is reasonable that the position of absorption bands in simulated UV-Vis and IR data are not exactly the same as experimental data.

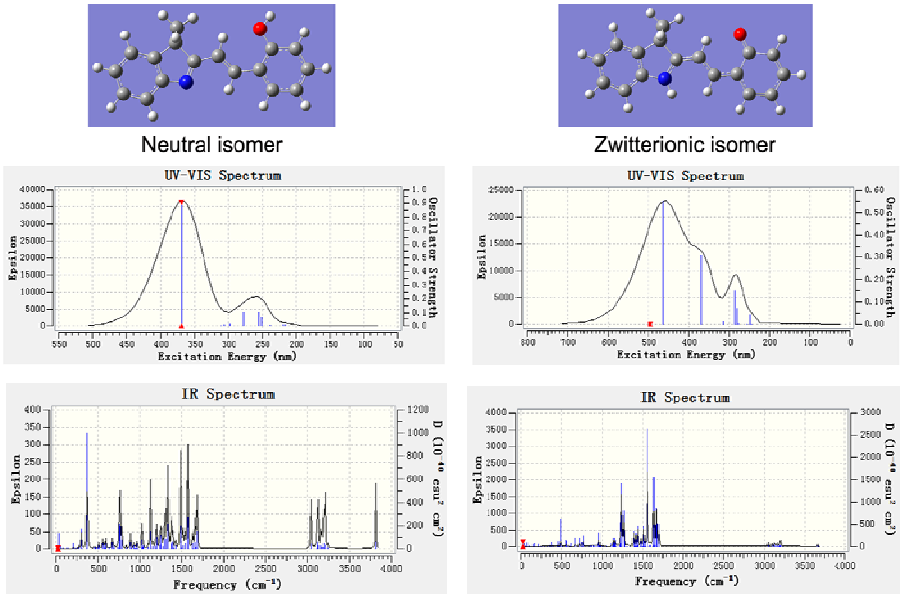

AM

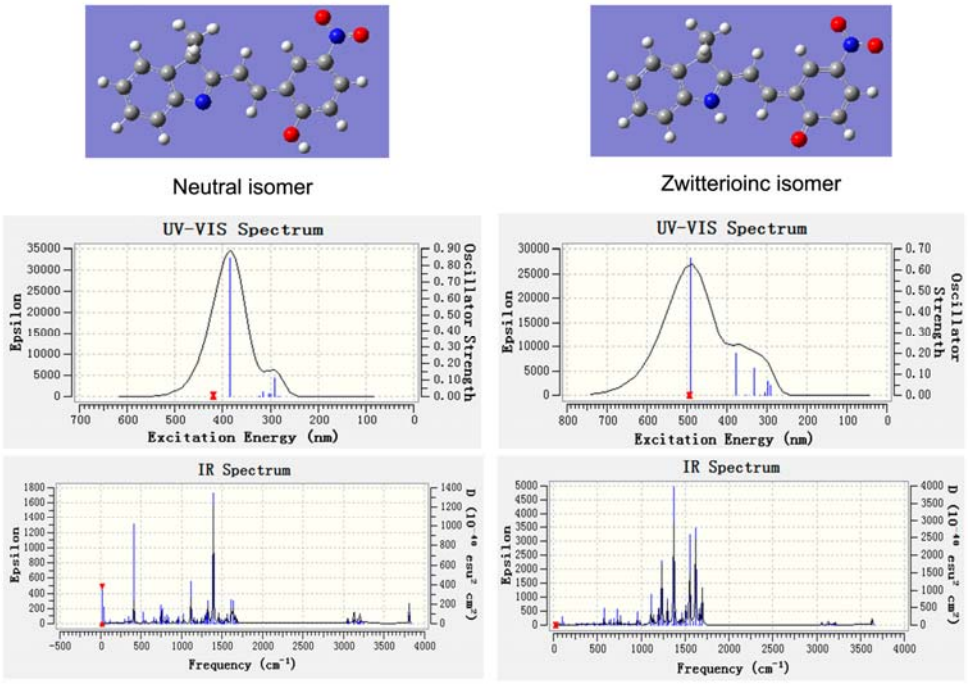

p-nitro-AM

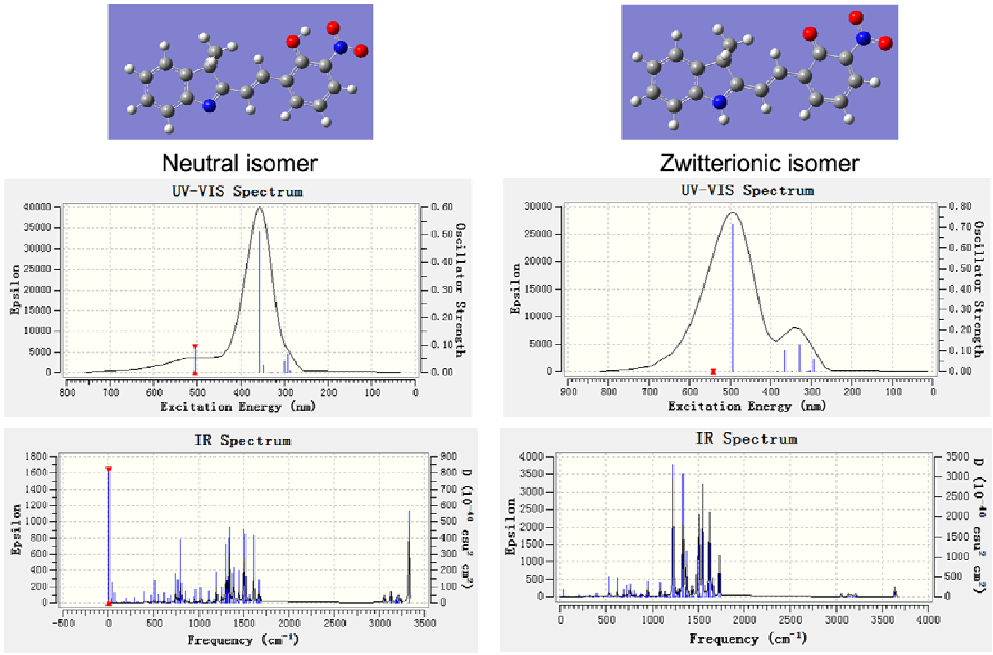

o-nitro-AM

Figure S2. Simulated total energies for the isolated neutral and zwitterionic isomers of **p-nitro-AM**. The simulation results show that the neutral isomer of an isolated **p-nitro-AM** in vacuum has better thermodynamics stability with 3.34 kcal·mol^{-1} lower in energy than that in its zwitterionic isomer, which explains why the zwitterionic isomer prefers to reverse back to neutral form after stress being released.

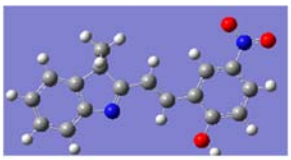

Neutral isomer

File Type	.log	
Calculation Type	FREQ	
Calculation Method	RB3LYP	
Basis Set	6-31G(d,p)	
Charge	0	
Spin	Singlet	
E(RB3LYP)	-1030.64822877	a.u.
RMS Gradient Norm	0.00000187	a.u.
Imaginary Freq	0	
Dipole Moment	3.4387	Debye
Point Group	C1	

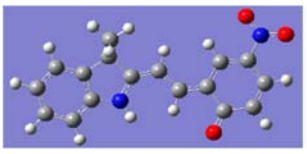

Zwitterionic isomer

File Type	.log	
Calculation Type	FREQ	
Calculation Method	RB3LYP	
Basis Set	6-31G(d,p)	
Charge	0	
Spin	Singlet	
E(RB3LYP)	-1030.64290161	a.u.
RMS Gradient Norm	0.00001733	a.u.
Imaginary Freq	0	
Dipole Moment	10.3533	Debye
Point Group	C1	

Table S2. Summary of crystal data and intensity collection parameters for **AM**, **p-nitro-AM** and **o-nitro-AM**.

Compound	**AM**	**p-nitro-AM**	**o-nitro-AM**
Formula	$C_{18}H_{17}NO$	$C_{18}H_{16}N_2O_3$	$C_{18}H_{16}N_2O_3$
Formula mass	263.33	308.33	308.33
Space group	P21/n	P21/n	P21/c
a/ Å	5.9589(12)	16.289(5)	8.578(5)
b/ Å	20.362(4)	5.772(5)	17.638(5)
c/ Å	12.149(2)	16.527(5)	10.333(5)
α/°	90	90.000(5)	90.000(5)
β/°	92.17(3)	92.596(5)	102.223(5)
γ/°	90	90.000(5)	90.000(5)
V/Å^3	1473.0(5)	1552.3(15)	1527.9(12)
Z	4	4	4
ρ/g.cm^{-3}	1.187	1.319	1.340
μ/mm^{-1}	0.073	0.744	0.093
F_{000}	560	648	648
Temp, (K)	293(2)	293(2)	293(2)
No. of collected reflns.	10953	8404	6867
No. of unique reflns.(R_{int})	2568(0.0380)	2702(0.0617)	3468(0.0189)
Data/restraints/parameters	2568 / 6 / 194	2702 / 0 / 208	3468 / 0 / 208
R_1, wR_2 [obs I > 2σ (I)]	0.0640, 0.1985	0.0591, 0.1641	0.0488, 0.1188
R_1, wR_2 (all data)	0.0947, 0.2310	0.0671, 0.1814	0.0698, 0.1315
Residual peak/hole e.Å^{-3}	0.342/-0.281	0.266/-0.264	0.173/-0.224
Goodness-of-fit on F^2	1.101	1.043	1.034

The crystal data for **AM**, **p-nitro-AM** and **o-nitro-AM** were deposited into Cambridge Crystallographic Data Centre with CCDC numbers of 895282, 895281, and 895283, respectively.

Figure S3. The dihedral angles between phenolic plane and indole plane for **AM**, **p-nitro-AM** and **o-nitro-AM** (the red plane represents for indole plane and the yellow plane represents for phenolic plane).

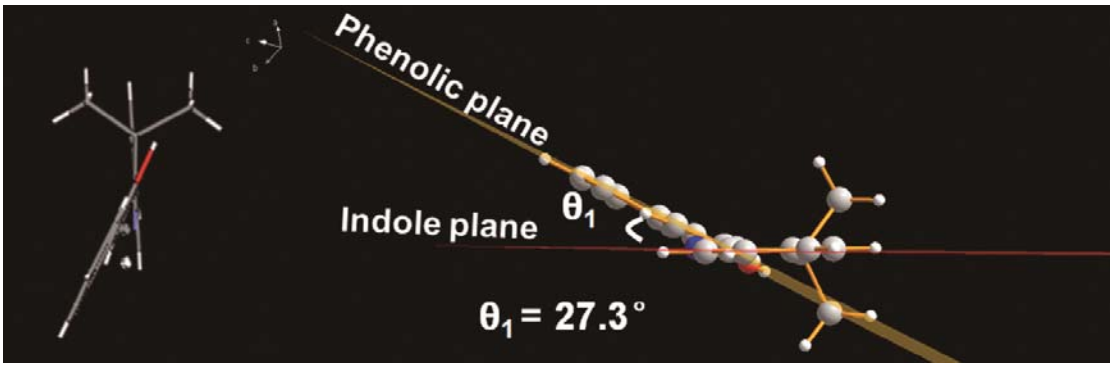

AM

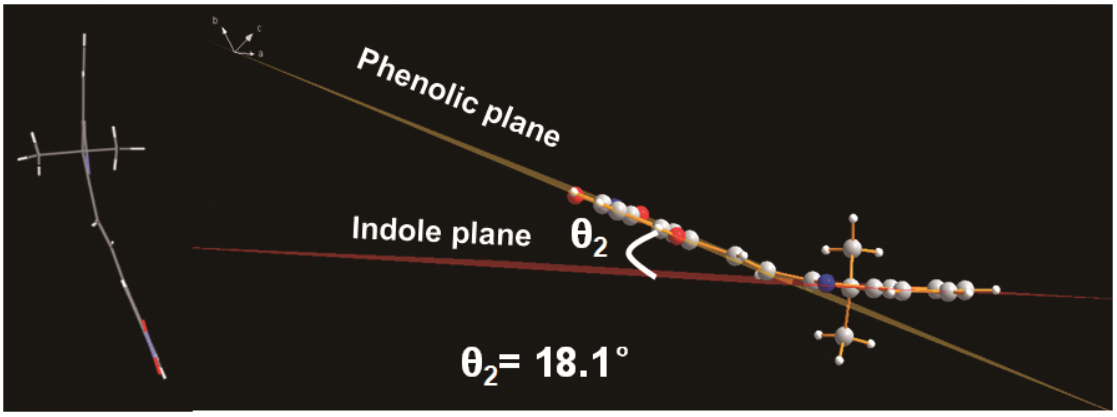

p-nitro-AM

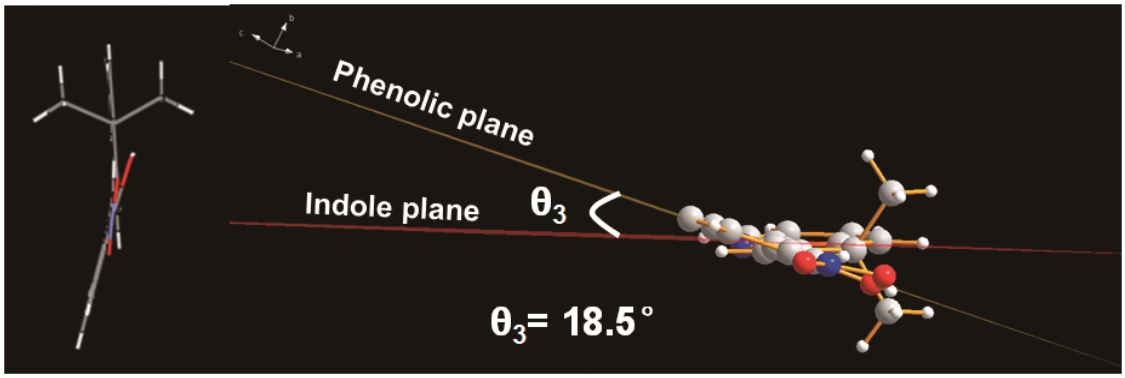

o-nitro-AM

3. Characterizations of AM, p-nitro-AM, o-nitro-AM and di-nitro-AM before and after grinding

Figure S4. (a) Optical microscopy images, (b) Kubelka-Munk diffuse reflectance absorption spectra, (c) emission spectra and (d) IR spectra of unground and ground **AM**. No obvious changes were observed in Figure S4a-4d, indicating proton transfer didn't occur.

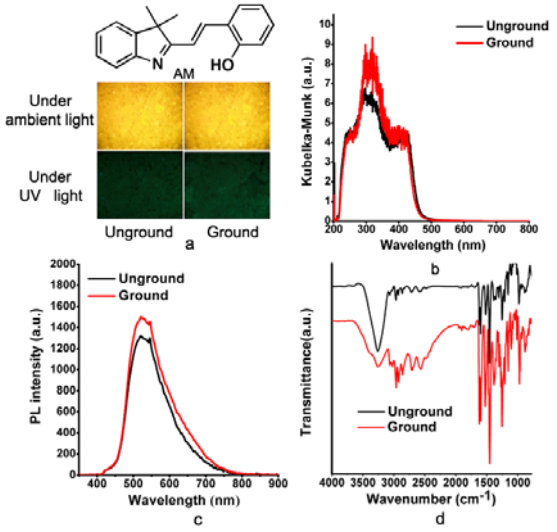

Figure S5. (a) Optical microscopy images, (b) Kubelka-Munk diffuse reflectance absorption spectra, (c) emission spectra and (d) IR spectra of unground and ground **o-nitro-AM**. No obvious changes were observed in Figure S5a-5d, indicating proton transfer didn't occur.

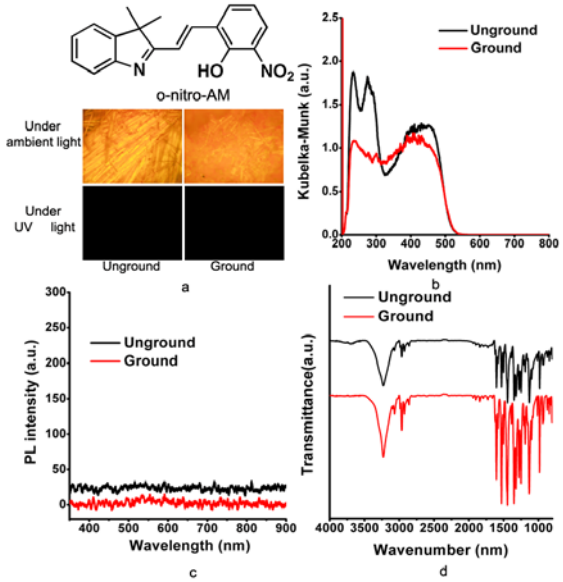

Figure S6. (a) Optical microscopy images, (b) Kubelka-Munk diffuse reflectance absorption spectra and (c) emission spectra of unground and ground **di-nitro-AM**; (d) IR spectra of unground **di-nitro-AM**. The almost disappearance of phenolic hydroxyl stretching absorption (3500 to 3200 cm^{-1}) and appearance of a broad stretching absorption band from 3100 to 2600 cm^{-1} by overlap of C−H stretching absorption of methyls in indole and N−H stretching absorption in $C=NH^{+}$ confirmed the zwitterionic form for **di-nitro-AM**.

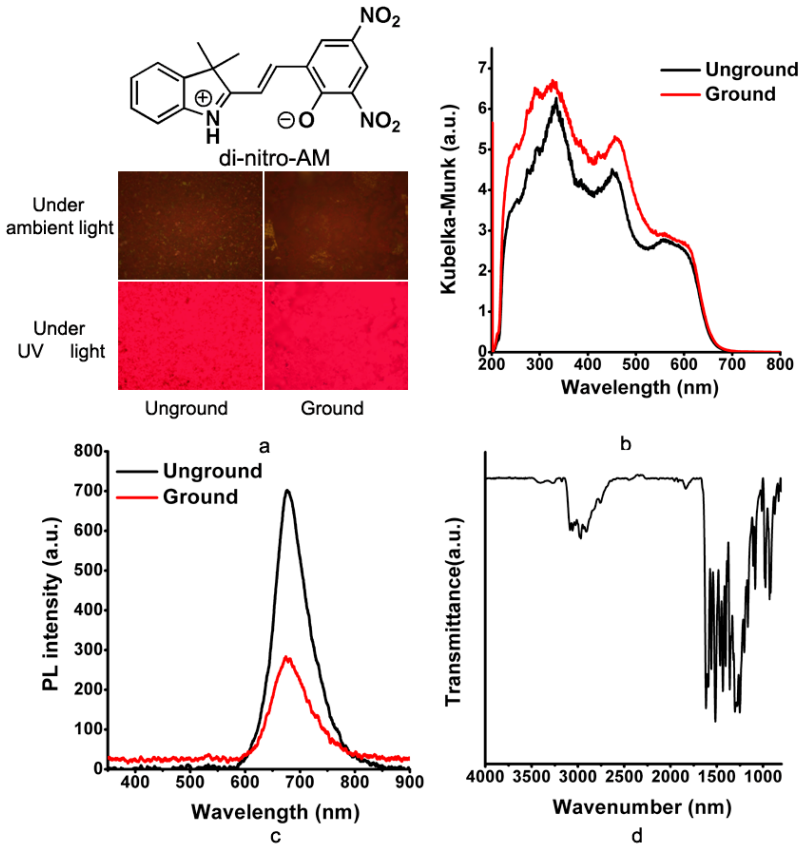

Figure S7. (a) The isomerization equilibrium of **p-nitro-AM** and **6-N-BIPS**; (b) absorption spectra of an ethanol solution of **6-N-BIPS** (1×10^{-5} M) under UV light irradiation (λ_{max} = 254 nm) for different times; (c) fluorescence spectra of an ethanol solution of **6-N-BIPS** (1×10^{-5} M) after UV light irradiation (λ_{max} = 365 nm) for 1.5 minutes.

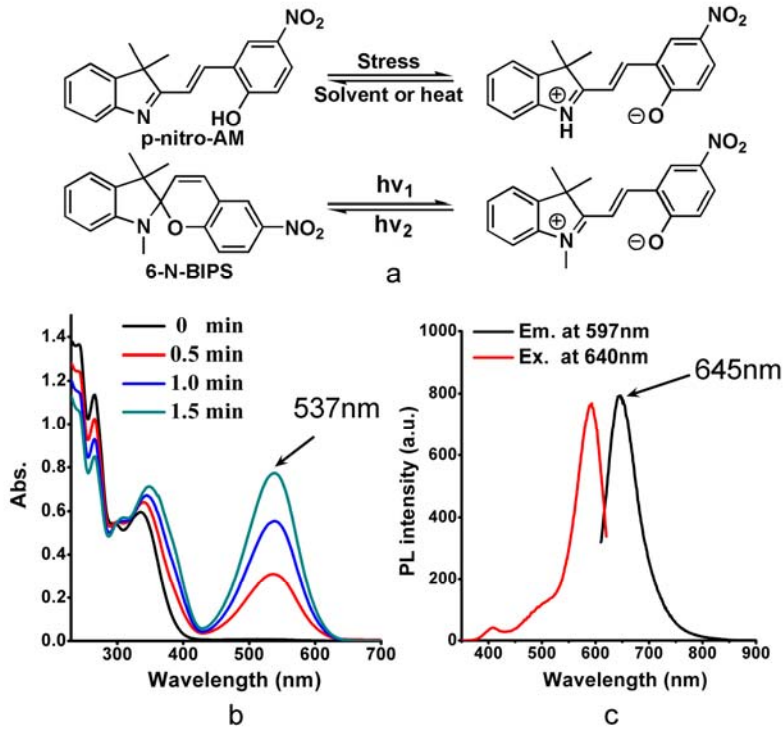

Figure S8. (a) XRD patterns, (b) N1s XPS spectra of **p-nitro-AM** in microcrystalline state, ground amorphous state and freeze-dried amorphous state (inset: the pictures of **p-nitro-AM** in microcrystalline state, ground amorphous state and freeze-dried amorphous states). XPS data suggested no zwitterionic **p-nitro-AM** was formed in freeze-dried amorphous state.

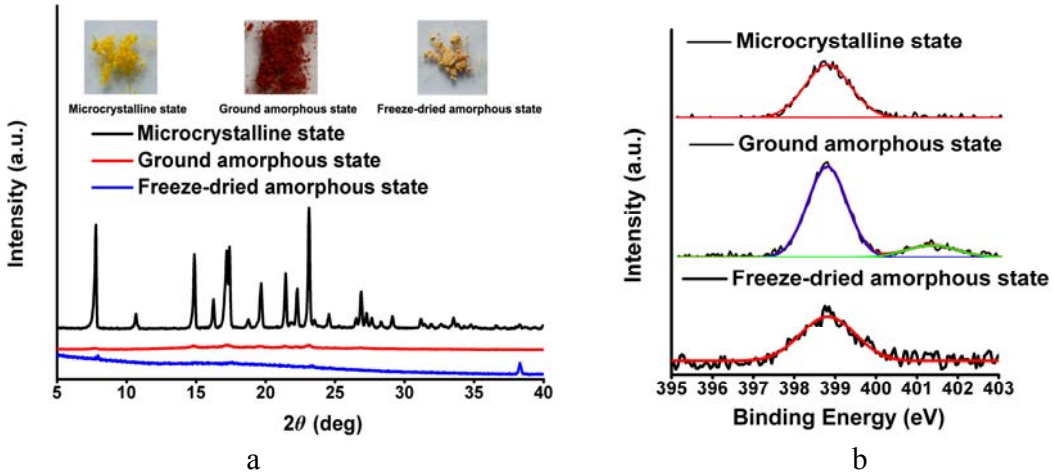

Figure S9. (a) Kubelka-Munk diffuse reflectance absorption spectra and microscopy images of **p-nitro-AM** under different static pressure for 5 minutes; (b) emission spectra and microscopy images of **p-nitro-AM** with different grinding time, indicating that 10MPa is enough to induce the proton transfer, and the neutral-to-zwitterionic transition ratio is dependent on the pressure and grinding time.

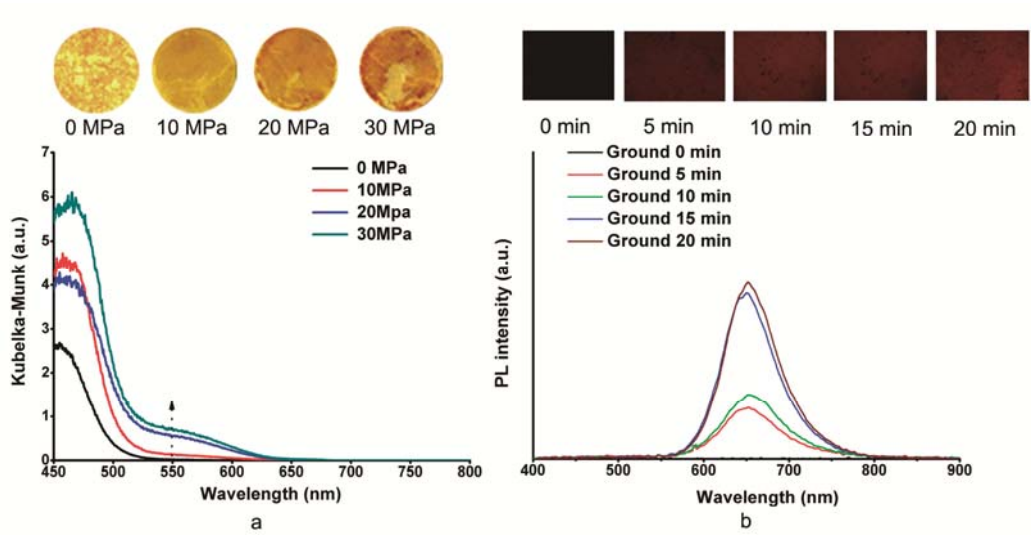

Figure S10. Rough estimation of neutral-to-zwitterionic transition ratio for **p-nitro-AM** upon grinding: (a) XPS analysis of N1s, (b) in-situ Kubelka-Munk diffuse reflectance absorption spectra and fluorescence spectroscopies and DSC curves for the ground sample and after stored for 20 hours.

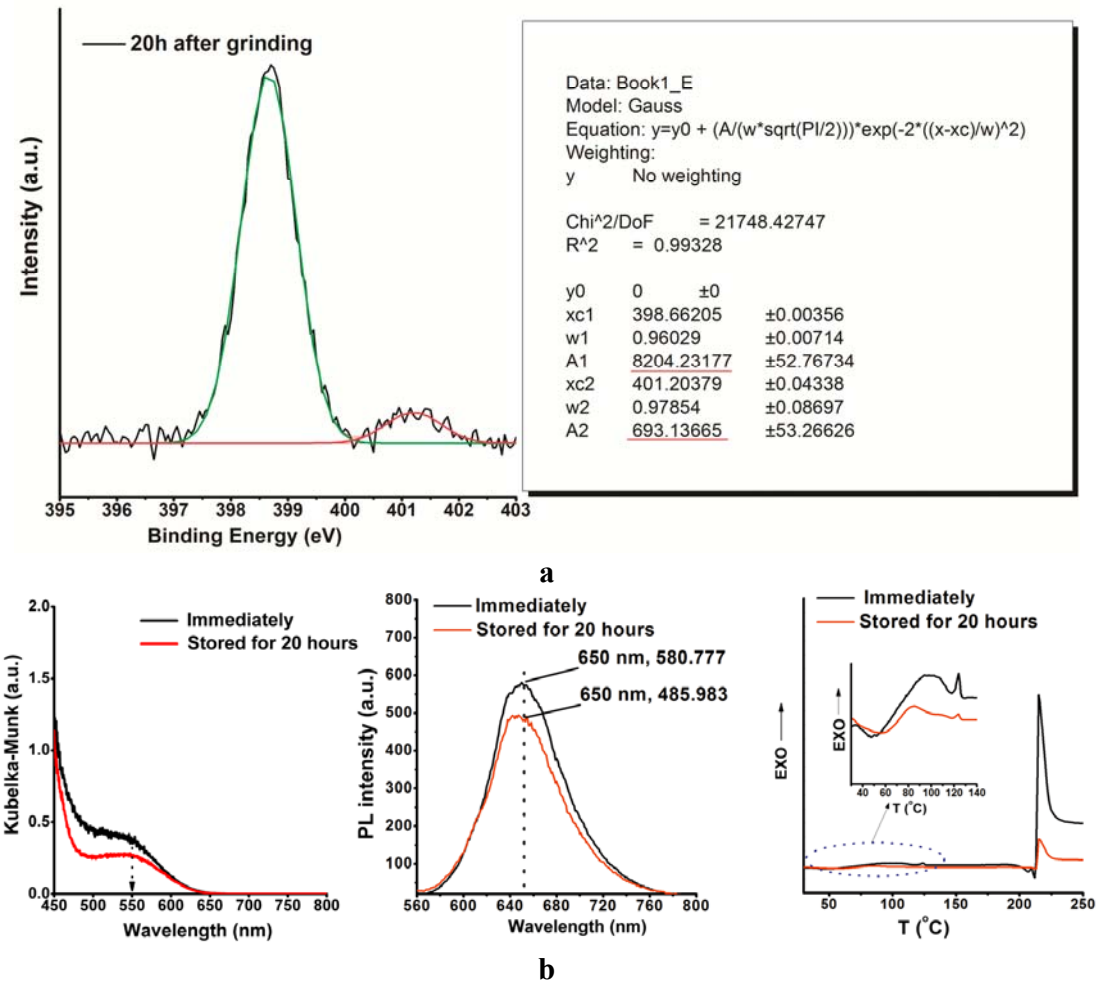

Because the proton-transfer results in an obvious shift in N1s binding energy of **p-nitro-AM**, N1s XPS spectrum was applied to estimate neutral-to-zwitterionic transition ratio. We supposed that the peak areas were proportional to their concentrations. The percentage of zwitterionic form was calculated to be 7.8 % (693 / (693+8204)) for the ground sample which had been hand-ground for about one hour and evacuated for 20 hours under ambient conditions before measurements (Figure S10a). To estimate how much zwitterionic isomer of **p-nitro-AM** turned back to neutral form during the 20 hours, the ground samples were subjected to in-situ Kubelka-Munk diffuse reflectance absorption and fluorescence spectra and DSC measurement immediately and after stored for 20 hours under ambient conditions. Owing to the absence of a direct correlation between the concentrations and Kubelka-Munk diffuse reflectance absorption spectra and the overlap of peaks involved in zwitterionic-to-neutral transition (from 30 °C to 150 °C) in DSC curve, in-situ fluorescence spectra was chosen for such an estimate. The fluorescent intensity of the stored sample was only 83.7 % (485.983 / 580.777) of that for the sample measured immediately (Figure S10b), which meant that there were 16.3% zwitterionic isomers reverted to neutral ones. So we could draw the conclusion hand-grinding could induce approximate 9.3 % (7.8 % / 83.7 %) neutral isomers to transform into zwitterionic ones.

4. Determination of pKa and pKb of AM, p-nitro-AM and o-nitro-AM by UV-Vis absorption spectra

If HB represents for an acid, there is following dissociation equilibrium: [6]

$$HB \rightleftharpoons B^- + H^+ \longrightarrow Ka = [B^-][H^+] / [HB] \cdots\cdots (1)$$

When the acid HB and its conjugate base B^- have an overlapped absorption at a selected wavelength, the absorbance at the selected wavelength can be expressed as follow:

$$A = A_{HB} + A_{B^-} = \varepsilon_{HB}[HB] + \varepsilon_{B^-}[B^-]$$

$$= \varepsilon_{HB} c_{HB} \frac{[H^+]}{Ka + [H^+]} + \varepsilon_{B^-} c_{HB} \frac{Ka}{Ka + [H^+]} \cdots\cdots (2)$$

When the pH values are low enough, the acid exists in only HB form, c_{HB} = [HB], $A_{HB} = \varepsilon_{HB} c_{HB}$. When the pH values are high enough, the acid exists only in B^- form, c_{B^-} = [HB], $A_{B^-} = \varepsilon_{B^-} c_{HB}$. But for a suitable pH range, there are HB form and B^- form existing in solution. The eq.2 can therefore be replaced as follow:

$$A = A_{HB} \frac{[H^+]}{Ka + [H^+]} + A_{B^-} \frac{Ka}{Ka + [H^+]} \cdots\cdots (3)$$

Finally, the pKa can be expressed as follow:

$$pKa = pH - \lg [(A_{HB} - A) / (A - A_{B^-})] \cdots\cdots (4)$$

(A: the absorbance of HB and B^- at a selected wavelength at suitable pH values that they co-exist; A_{HB}: the absorbance of HB at the selected wavelength at pH values that only HB form exists; A_{B^-}: the absorbance of B^- at the selected wavelength at pH values that only B^- form exists)

If B represents for a base, there is following dissociation equilibrium:

$$B + H^+ \rightleftharpoons BH^+ \longrightarrow Kb = [BH^+] / [B][H^+] \cdots\cdots (5)$$

Similarly, the pKb can be expressed as follow:

$$pKb = pKw - pH + \lg [(A - A_{HB^+}) / (A_B - A)] \cdots\cdots (6)$$

(A: the absorbance of B and BH^+ at a selected wavelength at suitable pH values that they co-exist; A_B: the absorbance of B at the selected wavelength at pH values that only B form exists; A_{BH^+}: the absorbance of BH^+ at the selected wavelength at pH values that only BH^+ form exists; pKw: the dissociation constant for H_2O, which was determined as 14 for present calculation according to literature[6c]).

The pH was regulated by adding HCl or NaOH aqueous solution, whose volume was lower 1% of the volume of measured solution.

Figure S11. (a) UV-Vis spectra of **AM** with increasing pH values; (b) UV-Vis spectra of **AM** with decreasing pH values (C = 1.24×10^{-5} mol/L, $V_{CH_3CH_2OH}$:V_{H_2O} = 2:1); (c) calculation of dissociation constant pKa of **AM** (A_{HB} = 0.330, A_{B^-} = 0.089, λ sel.= 361 nm); (d) calculation of dissociation constant pKb of **AM** (A_B = 0.330, A_{BH^+} = 0.141, λ sel. = 361 nm).

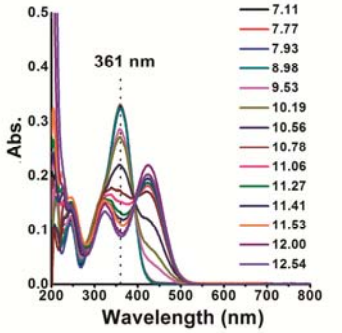

a

pH	A	$\lg\frac{A_{HB}-A}{A-A_{B^-}}$	pKa	Average
7.11	0.330			
10.19	0.270	-0.480	10.670	
10.56	0.219	-0.069	10.629	
10.78	0.171	0.288	10.492	10.586
11.06	0.152	0.451	10.609	
11.27	0.131	0.675	10.595	
11.41	0.121	0.815	10.595	
11.53	0.110	1.020	10.510	
12.54	0.089			

c

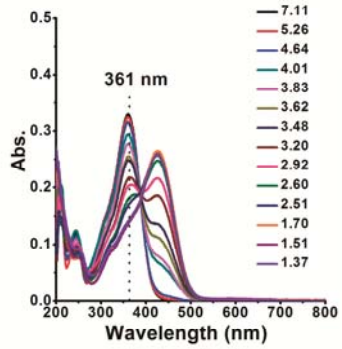

b

pH	A	$\lg\frac{A_B-A}{A-A_{BH^+}}$	pKb	Average
7.11	0.330			
5.26	0.324	-1.484	10.224	
4.64	0.315	-1.064	10.424	
4.01	0.293	-0.614	10.604	
3.83	0.276	-0.398	10.568	
3.62	0.255	-0.182	10.562	
3.48	0.248	-0.116	10.636	10.605
3.20	0.216	0.176	10.624	
2.92	0.202	0.322	10.758	
2.60	0.178	0.614	10.786	
2.51	0.169	0.760	10.730	
2.04	0.150	1.222	10.738	
1.70	0.141			

d

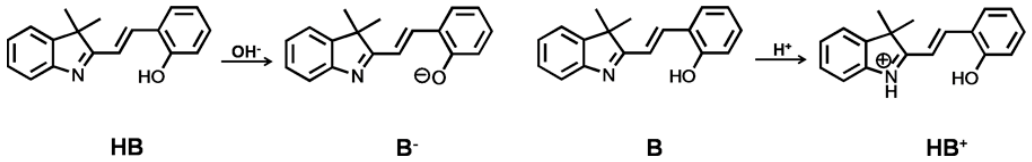

HB B⁻ B HB^+

Note: No matter NaOH or HCl aqueous solution was added to the solution of **AM**, a new peak around 450 nm appeared, which was assigned to deprotonated **AM** (B^-) or protonated **AM** (BH^+), respectively (Figure S11a and S11b). Without adding acid or base, the absence of the peak around 450 nm of **AM** indicated that it took a neutral form in the mixed solution ($V_{CH_3CH_2OH}$:V_{H_2O} = 2:1). So A_{HB} for pKa calculation and A_B for pKb calculation were defined as 0.330 at 361 nm. The absorbance of the peak at 361 nm decreased with the increasing pH values, indicating the formation of deprotonated **AM** (B^-) upon adding NaOH aqueous solution. When pH value was 12.54, the peak at 361 nm reached the minimum with a value of 0.089, which was defined as A_{B^-}. Similarly, when pH value was 1.70, the absorption at 361 nm reached the minimum with a value of 0.141, which was defined as A_{BH^+}.

Figure S12. (a) UV-Vis spectra of **p-nitro-AM** with increasing pH values (C = 1.16× 10^{-4} mol/L, $V_{CH_3CH_2OH}$:V_{H_2O} = 2:1); (b) UV-Vis spectra of **p-nitro-AM** with decreasing pH values (C = 1.18×10^{-4} mol/L, $V_{CH_3CH_2OH}$:V_{H_2O} = 2:1); (c) calculation of dissociation constant pKa of **p-nitro-AM** (A_{HB} =0, A_{B^-} = 2.929, λsel. = 436 nm); (d) calculation of dissociation constant pKb of **p-nitro-AM** (A_B = 2.953, A_{BH^+} = 1.599, λsel. = 353 nm).

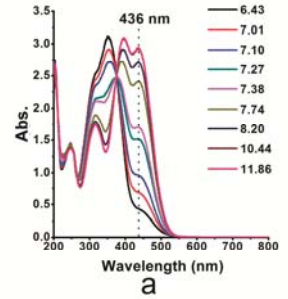

a

pH	A	$\lg\frac{A_{HB}-A}{A-A_{B^-}}$	pKa	Average
6.43	0.439	-0.754	7.184	
7.01	0.690	-0.511	7.521	
7.10	0.966	-0.308	7.408	
7.27	1.519	-0.031	7.238	7.252
7.38	1.705	0.144	7.236	
7.74	2.410	0.667	7.073	
8.20	2.711	1.095	7.105	
10.44	2.929			

c

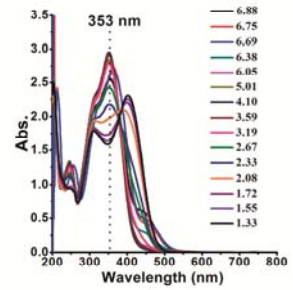

b

pH	A	$\lg\frac{A_B-A}{A-A_{BH^+}}$	pKb	Average
4.10	2.953			
3.59	2.918	-1.576	11.986	
3.19	2.795	-0.879	11.689	
2.67	2.420	-0.188	11.518	
2.33	2.174	0.132	11.538	11.515
2.08	1.978	0.410	11.510	
1.72	1.736	0.949	11.331	
1.55	1.649	1.416	11.034	
1.33	1.599			

d

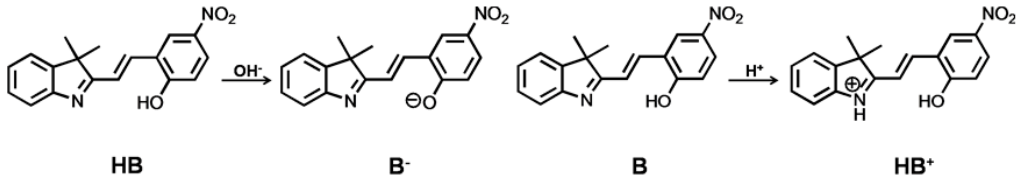

Notes: The shoulder peak at 436 nm of **p-nitro-AM** without adding acid or base (Figure S12a) indicated that the phenolic hydroxyl was partly dissociated to form deprotonated **p-nitro-AM** (B^-) in the mixed solution ($V_{CH_3CH_2OH}$:V_{H_2O} = 2:1). When HCl aqueous solution was added, the shoulder peak decreased first, accompanied with an absorbance increase of the peak at 353 nm (Figure S12b). Then an absorbance decrease of the peak at 353 nm continued with lowering pH values, which indicated that the deprotonated **p-nitro-AM** (B^-) was protonated first, followed by the nitrogen atom in indole in a lowing pH trend. The peak at 436 nm, which represented for the absorbance of only basic B^- form, was selected to calculate pKa. The absorbance was zero when it was not dissociated (A_{HB} = 0), and it changed to 2.929 when it was totally dissociated (A_{B^-} = 2.929). Similarly, the peak at 353 nm was selected to calculate pKb. The peak at 353 nm reached the maximum when pH value was 4.10 indicating the total formation of neutral **p-nitro-AM** (B), so it was defined as A_B. When pH value was 1.33, the peak at 353 nm reached the minimum, it was defined as A_{BH^+}.

Figure S13. (a) UV-Vis spectra of **o-nitro-AM** with increasing pH values; (b) UV-Vis spectra of **o-nitro-AM** with decreasing pH values (C =1.92×10^{-5} mol/L, $V_{CH_3CH_2OH}$:V_{H_2O} = 2:1); (c) calculation of dissociation constant pKa of **o-nitro-AM** (A_{HB} = 0.481, A_{B^-} = 0.191, $\lambda_{sel.}$ = 328 nm); (d) calculation of dissociation constant pKb of **o-nitro-AM** (A_B = 0.481, A_{BH^+} = 0.234, $\lambda_{sel.}$ = 328 nm).

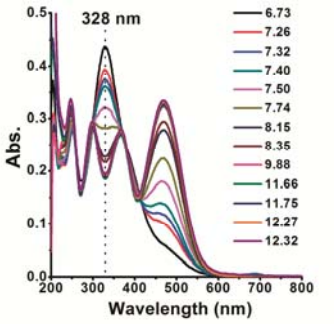

a

pH	A	$\lg\frac{A_{HB}-A}{A-A_{B^-}}$	pKa	Average
5.30	0.481			
7.26	0.394	-0.368	7.628	
7.32	0.376	-0.246	7.666	
7.40	0.362	-0.157	7.557	
7.50	0.322	0.084	7.426	7.480
7.74	0.283	0.333	7.407	
8.15	0.228	0.835	7.312	
8.35	0.218	0.988	7.362	
12.32	0.191			

c

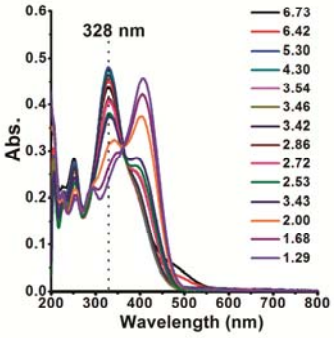

b

pH	A	$\lg\frac{A_B-A}{A-A_{BH^+}}$	pKb	Average
5.30	0.481			
4.30	0.474	-1.535	11.235	
3.46	0.465	-1.159	11.699	
2.86	0.412	-0.412	11.552	
2.72	0.405	-0.352	11.632	11.612
2.53	0.380	-0.160	11.630	
2.43	0.372	-0.102	11.672	
2.00	0.311	0.344	11.656	
1.68	0.263	0.876	11.444	
1.29	0.234			

d

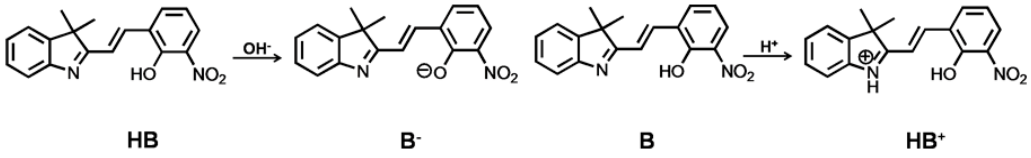

HB B^- B HB^+

Note: Similar to **p-nitro-AM**, **o-nitro-AM** was also partly dissociated to form deprotonated **o-nitro-AM** (B^-) in the mixed solution ($V_{CH_3CH_2OH}$:V_{H_2O} = 2:1) (Figure S13a). And it also exhibited the characteristic that the partly deprotonated **o-nitro-AM** (B^-) was protonated first, followed by the nitrogen atom in indole in a lowing pH trend (Figure S13b). When the pH value was 5.30, the shoulder peak at 469 nm disappeared and the peak at 328 nm reached maximum, indicating the total formation of neutral **o-nitro-AM**, which was defined as A_{HB} for pKa calculation and A_B for pKb calculation. When pH value was 12.32, the peak at 328 nm reached the minimum, it was defined as A_{B^-}. When pH value was 1.29, the peak at 328 nm reached the minimum, it was defined as A_{BH^+}.

5. ^{1}H NMR and ^{13}C NMR of AM, p-nitro-AM, o-nitro-AM, di-nitro-AM and 6-N-BIPS

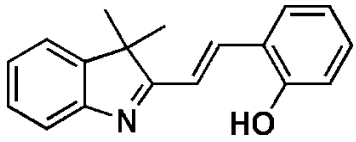

AM

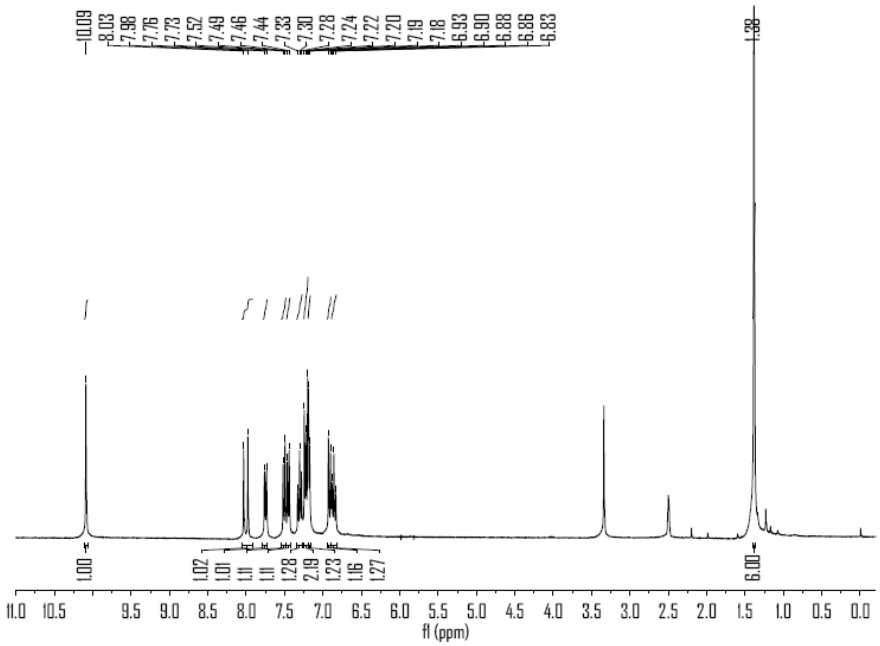

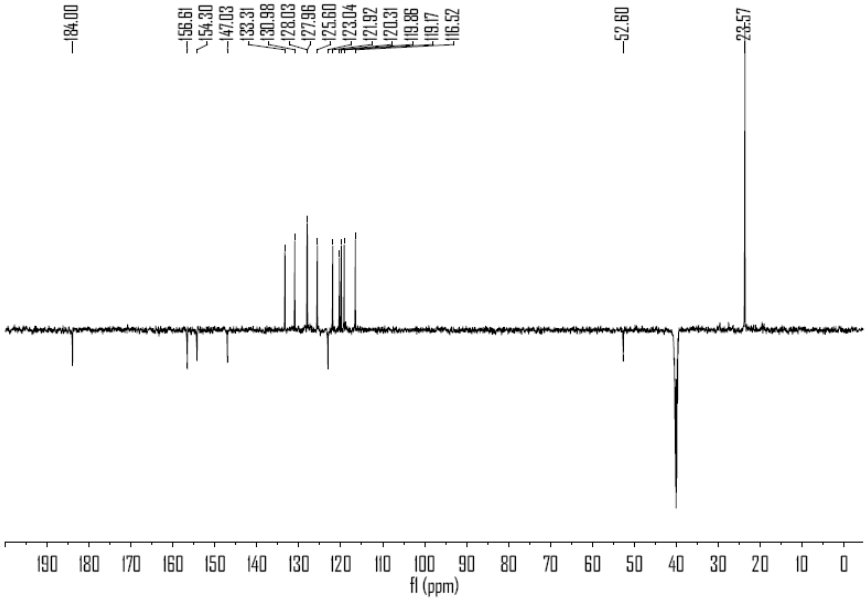

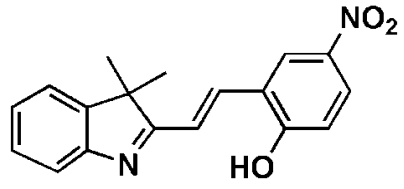
NO2
N
HO

p-nitro-AM

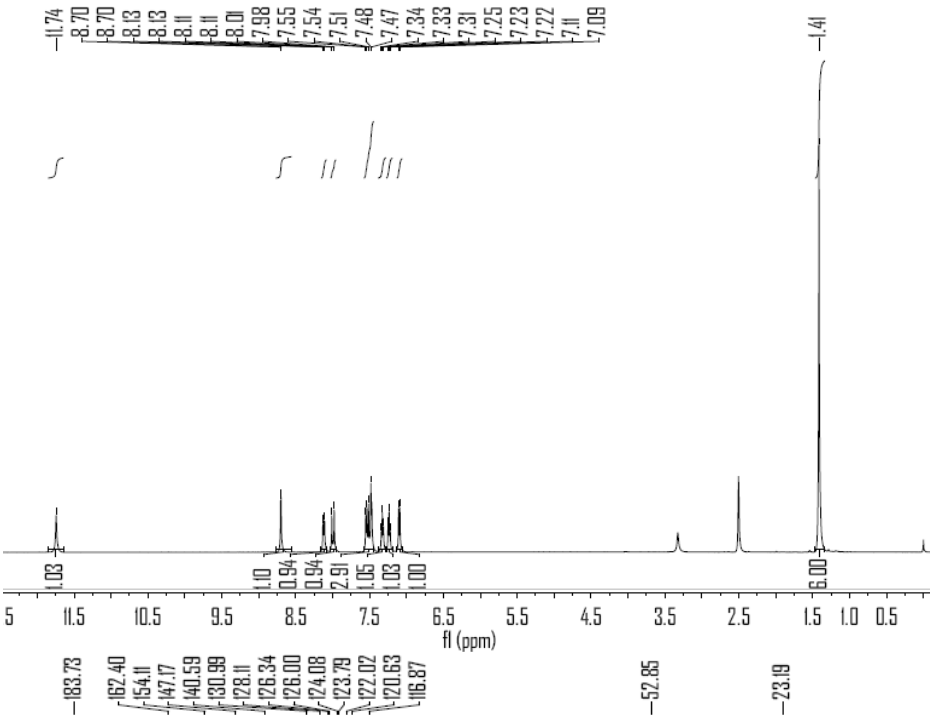
11.74
8.70
8.70
8.13
8.13
8.11
8.11
8.01
7.98
7.55
7.54
7.51
7.48
7.47
7.34
7.33
7.31
7.25
7.23
7.22
7.11
7.09
1.41
1.03
1.10
0.94
0.94
2.91
1.05
1.03
1.00
6.00
f1 (ppm)
183.73
162.40
154.11
147.17
140.59
130.98
128.11
126.34
126.00
124.08
123.79
122.02
120.63
116.87
52.85
23.19
f1 (ppm)

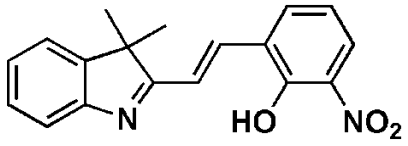
N
HO
NO2

o-nitro-AM

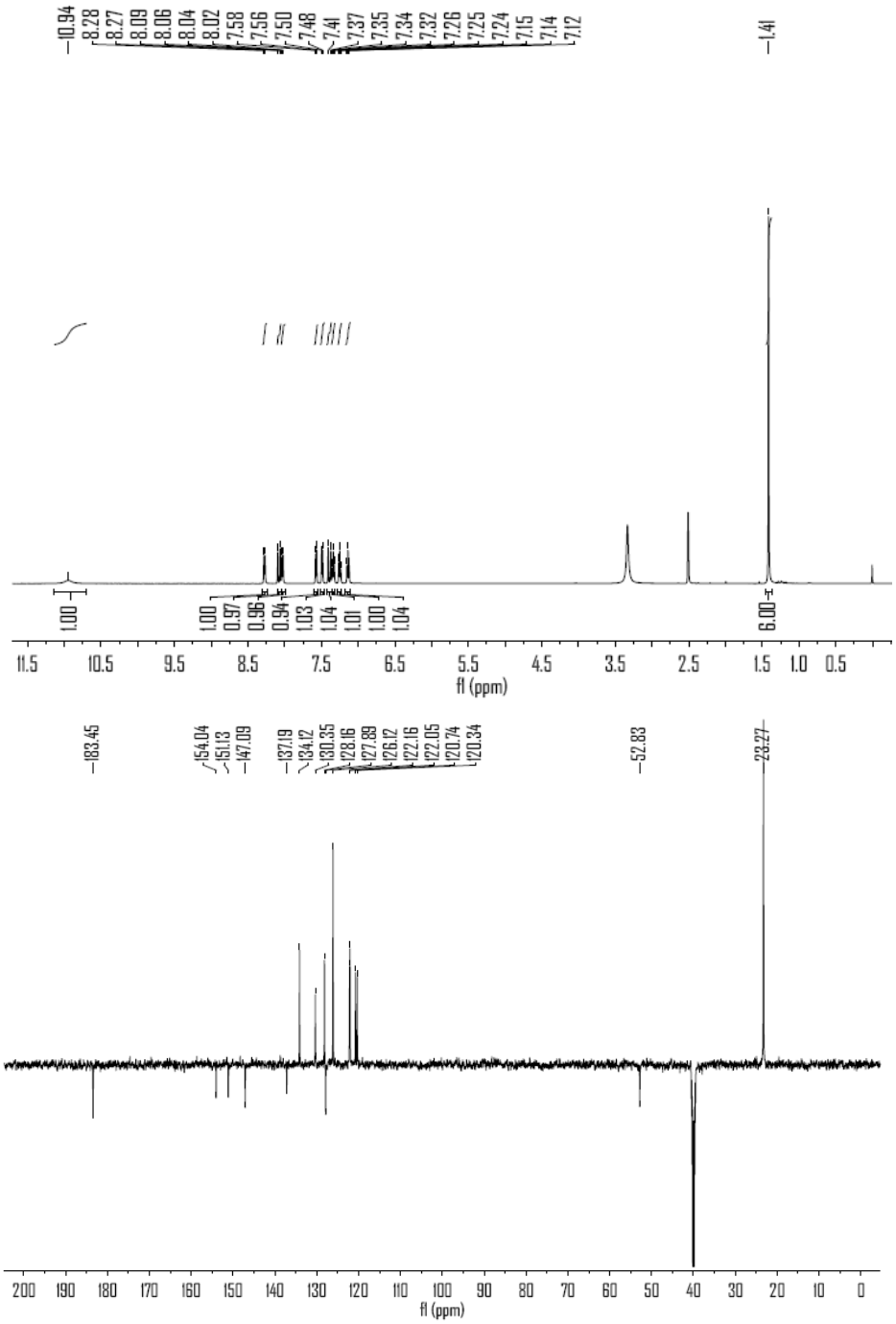
10.94
8.28
8.27
8.09
8.06
8.04
8.02
7.58
7.56
7.50
7.48
7.41
7.37
7.35
7.34
7.32
7.26
7.25
7.24
7.15
7.14
7.12
1.41
1.00
1.00
0.97
0.96
0.94
1.03
1.04
1.01
1.00
1.04
6.00
11.5
10.5
9.5
8.5
7.5
6.5
5.5
4.5
3.5
2.5
1.5
1.0
0.5
f1 (ppm)
183.45
154.04
151.13
147.09
137.19
134.12
130.35
128.16
127.88
126.12
122.16
122.05
120.74
120.34
52.83
23.27
200
190
180
170
160
150
140
130
120
110
100
90
80
70
60
50
40
30
20
10
0
f1 (ppm)

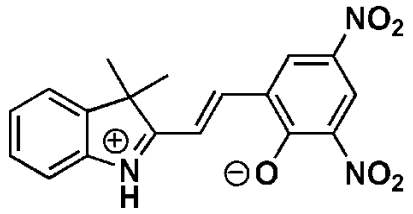
NO2
NO2
O
N
H

di-nitro-AM

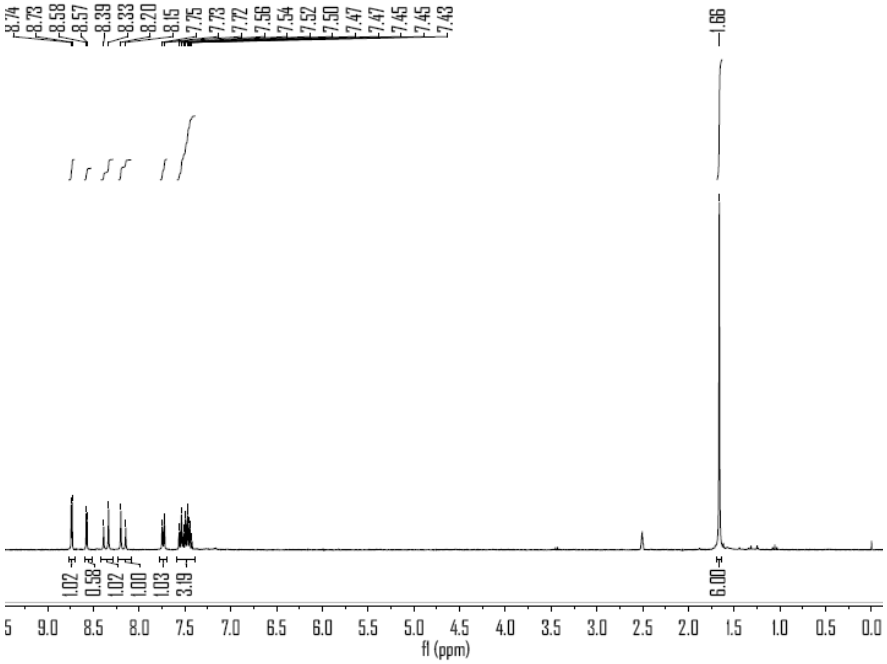
8.74
8.73
8.58
8.57
8.39
8.33
8.20
8.15
7.75
7.73
7.72
7.56
7.54
7.52
7.50
7.47
7.47
7.45
7.45
7.43
1.66
1.02
0.58
1.02
1.00
1.03
3.19
6.00
f1 (ppm)

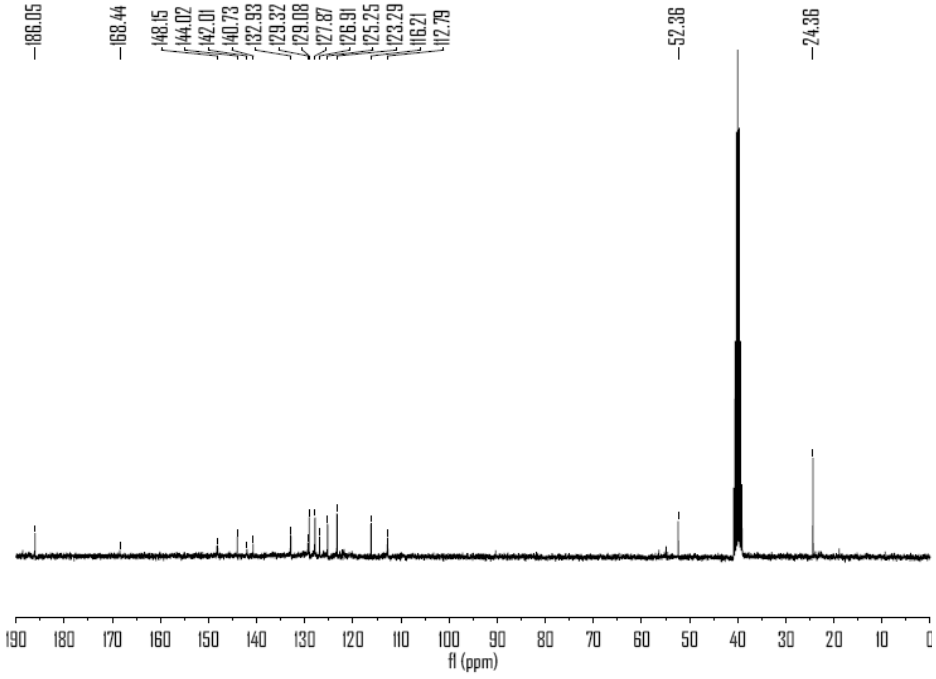
186.05
168.44
148.15
144.02
142.01
140.73
132.93
129.32
129.08
127.87
126.91
125.25
123.29
116.21
112.79
52.36
24.36
f1 (ppm)

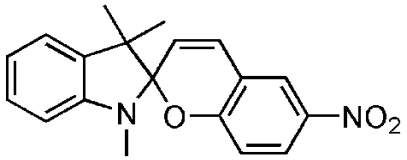
N
O
NO2

6-N-BIPS

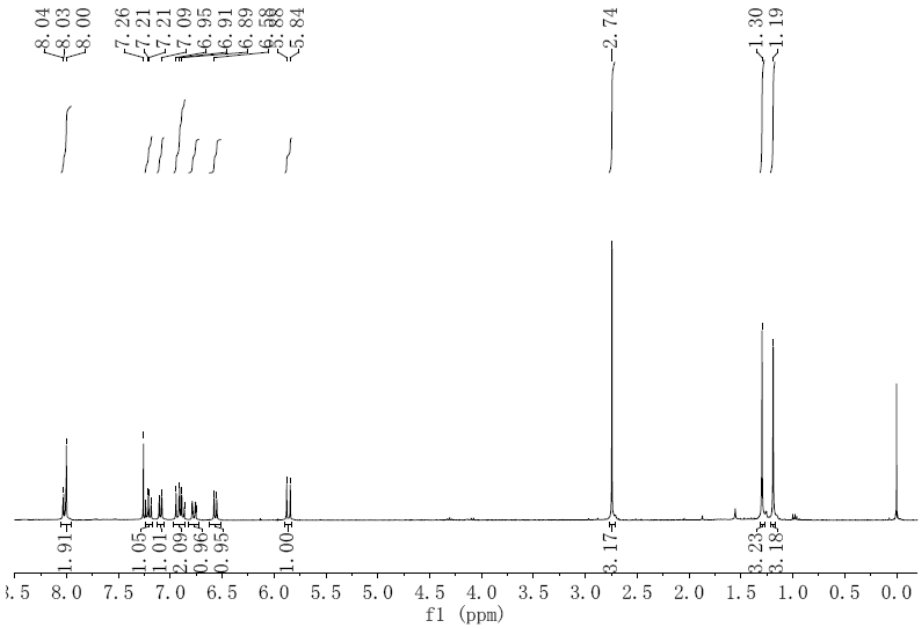
8.04
8.03
8.00
7.26
7.21
7.21
7.09
6.95
6.91
6.89
6.58
6.58
5.84
2.74
1.30
1.19
1.91
1.05
1.01
2.09
0.96
0.95
1.00
3.17
3.23
3.18
f1 (ppm)

References

1 (a) C. J. Roxburgh, P. G. Sammes and A. Abdullah, *Dyes Pigm.,* 2009, **83**, 31; (b) Y. Zhang, H. Zhang, J. Li and X. Lu , *Dyestuffs and coloration* 2005, **42**, 38; (c) H. Zhang, X. Niu, Y. Shi, Y. Liu and Z. Li, *Chinese Journal of New Drugs* 2008, **17**, 303.

2 (a) P. Kubelka and F. Z. Munk, *Technol. Phys.*, 1931, **12**, 593; (b) P. Kubelka, *J. Opt. Soc. Am.*, 1947, **38**, 448; (c) R. S. Agam, W. L. Joseph, J. M. Eric, X. M. Francis and J. W. G. David, *J. Am. Chem. Soc.*, 2005, **127**, 6641.

3 A. E. Reed, L. A. Curtiss and F. Weinhold, *Chem. Rev.,* 1988, **88**, 899.

4 M. J. Frisch, G. W. Trucks, H. B. Schlegel, G. E. Scuseria, M. A. Robb, J. R. Cheeseman, G. Scalmani, V. Barone, B. Mennucci, G. A. Petersson, H. Nakatsuji, M. Caricato, X. Li, H. P. Hratchian, A. F. Izmaylov, J. Bloino, G. Zheng, J. L. Sonnenberg, M. Hada, M. Ehara, K. Toyota, R. Fukuda, J. Hasegawa, M. Ishida, T. Nakajima, Y. Honda, O. Kitao, H. Nakai, T. Vreven, J. Montgomery, J. A. , J. E. Peralta, F. Ogliaro, M. Bearpark, J. J. Heyd, E. Brothers, K. N. Kudin, V. N. Staroverov, R. Kobayashi, J. Normand, K. Raghavachari, A. Rendell, J. C. Burant, S. S. Iyengar, J. Tomasi, M. Cossi, N. Rega, J. M. Millam, M. Klene, J. E. Knox, J. B. Cross, V. Bakken, C. Adamo, J. Jaramillo, R. Gomperts, R. E. Stratmann, O. Yazyev, A. J. Austin, R. Cammi, C. Pomelli, J. W. Ochterski, R. L. Martin, K. Morokuma, V. G. Zakrzewski, G. A. Voth, P. Salvador, J. J. Dannenberg, S. Dapprich, A. D. Daniels, O. Farkas, J. B. Foresman, J. V. Ortiz, J. Cioslowski, and D. J. Fox, *Gaussian 09, (Revision A. 02), Gaussian, Inc., Wallingford, CT* **2009**.

5 Y. Shiraishi, K. Adachi, M. Itoh and T. Hirai, *Org. Lett.,* 2009, **11**, 3482.

6 (a) S. Miltsov, C. Encinas and J. Alonso, *Tetrahedron Lett.,* 1999, **40**, 4067; (b) M. S. Briggs, D. D. Burns, M. E. Cooper and S. J. Gregory, *Chem. Commun.,* 2000, 2323; (c) S. Zhang and X. Zhang, *Chemical Reagents* 2009, **31**, 115.